Proceedings of the Combustion Institute 40 (2024) 105309

Contents lists available at ScienceDirect

Proceedings of the Combustion Institute

journal homepage: www.elsevier.com/locate/proci

Carrier-phase direct numerical simulation and flamelet modeling of alkali metal emissions from pulverized biomass flames

Ali Shamooni [a,*,1], Xu Wen [b,c,1], Paulo Debiagi [c,d], Alessandro Stagni [e], Jan W. Gärtner [a], Thorsten Zirwes [a], Oliver T. Stein [f], Christan Hasse [c], Andreas Kronenburg [a]

[a] Institute for Combustion Technology (ITV), University of Stuttgart, Pfaffenwaldring 31, 70569 Stuttgart, Germany
[b] State Key Laboratory of Fire Science, University of Science and Technology of China, Huangshan Road 443, 230026 Hefei, PR China
[c] Simulation of Reactive Thermo-Fluid Systems (STFS), TU Darmstadt, Otto-Berndt-Straße 2, 64287 Darmstadt, Germany
[d] Nottingham Ningbo China Beacons of Excellence Research and Innovation Institute, University of Nottingham Ningbo China, Ningbo 315100, PR China
[e] Department of Chemistry, Materials, and Chemical Engineering, Politecnico di Milano, Piazza Leonardo da Vinci 32, 20133 Milano, Italy
[f] Engler-Bunte-Institut, Simulation of Reacting Thermo-Fluid Systems, Karlsruhe Institute for Technology, Engler-Bunte-Ring 7, 76131 Karlsruhe, Germany

ARTICLE INFO

Keywords:
Pulverized biomass combustion
Alkali metal emissions
Carrier-phase DNS
Flamelet modeling
Oxy-fuel combustion

ABSTRACT

Combustion of biomass, as a CO_2-neutral and renewable fuel, is an appealing option in transition to sustainable energy sources. However, biomass combustion is prone to generate harmful alkali metals and corresponding sulfates. In this study, we analyze the potassium-containing species emissions in the early stages of turbulent pulverized biomass combustion (PBC) in an oxy-fuel atmosphere. To this end, a 3D carrier-phase direct numerical simulation of pulverized walnut shells combustion is carried out. A realistic fuel composition including heavy tars, obtained by the state-of-the-art CRECK-S-B model, KOH, KCl, and SO_2 is considered and detailed homogeneous kinetics for both hydrocarbons and K-Cl-S containing species is employed. The DNS results show that in the considered conditions, the flame is predominantly non-premixed in the vicinity of the stoichiometric surface, while in richer regions, in the center of the turbulent jet, a mix of premixed and non-premixed combustion modes is prevalent. Potassium sulfate (K_2SO_4) forms in a high amount in a fuel-rich and strained region in the center of the jet, mainly through the direct reaction of K-radicals with SO_2. The chemical time scale analysis reveals the slow processes of KOH consumption and K_2SO_4 production in this region. Closer to the flame surface, K_2SO_4, KCl, and KOH are consumed which lead to the production of K and KO_2. The predictions from a flamelet/progress variable approach are compared to the DNS data. Overall, the predictions of the flamelet model based on steady non-premixed flamelets are satisfactory. Specifically, temperature, light hydrocarbon species, and Cl-containing species (HCl and KCl) are well predicted across the jet flame. A major tar species ($C_8H_8O_3$), K, KOH, and K_2SO_4 predictions show discrepancies with the DNS data in the center of the jet, which can be related to the slow kinetics of these species and a mixed combustion mode in this region.

1. Introduction

The combustion of fossil fuels is associated with an unsustainable carbon footprint, which can be mitigated by the combustion of CO_2-neutral biomass.

A practical challenge in pulverized biomass combustion (PBC) is the deposition of alkali compounds and corrosion due to the high content of alkali metals such as potassium (K) and elements such as chlorine (Cl) in the ash or flue gases [1]. Depending on the biomass type and its ash composition, it can be rich in elements K, Cl, silica (Si), and sulfur (S), the ratio and interaction of which affect the concentration of released potassium compounds and the degree of further sulfation [2,3]. The sulfates and alkali salts that are formed due to interactions of S- and K-containing species (hereafter S- and K-species) may further nucleate in cooling environments, form sticky deposits, and/or be released as aerosols into the atmosphere, with severe environmental impacts [1,3,4].

Experiments were carried out on different biomass types to identify the release forms and mechanisms of alkali species and to quantify them [2,4–7]. It was found that the potassium content of biomass can be released in the forms of gaseous K, KOH, KCl but the amounts highly depend on the biomass type, e.g., the ratio of K to silica and/or

* Corresponding author.
E-mail addresses: ali.shamooni@polimi.it, ali.shamooni@itv.uni-stuttgart.de (A. Shamooni).
[1] Equal contributions.

https://doi.org/10.1016/j.proci.2024.105309
Received 4 December 2023; Accepted 31 May 2024
Available online 26 July 2024

chlorine [2,7], and the surrounding composition [5]. Similarly, the specific released compounds containing Cl and S depend on the biomass type and environment [2]. Possible reaction paths of vaporized K-species and their interaction with Cl- and S-containing species have been identified [3,4,6] which resulted in detailed gas-phase K-Cl-S species sub-mechanisms.

Unlike the numerous existing experiments, there are no extensive numerical analyses of the emissions of alkali metals in PBC. Ma et al. [8] numerically investigated K release during combustion of pulverized wood in a 1 MW industrial furnace with a simplified KOH release and gas-phase oxidation mechanisms. Mousavi et al. [9] considered a high silica (K/Si $\approx$ 1), low Cl (K/Cl $\gg$ 1) biomass and numerically studied the release of gas-phase K-species inside a 140 kW entrained flow gasifier. While they used a multi-step K-release mechanism, a global gas-phase reaction mechanism was employed.

The computational cost of employing detailed chemistry motivates the use of tabulation methods. Flamelet modeling approaches have been extensively used for pulverized coal combustion (PCC) simulations and have shown their advantages, as detailed chemistry can be included in simulations at a relatively low cost by pre-tabulation of premixed/non-premixed flamelets [10]. The application of flamelet models for PBC is, however, in a developing stage [11]. In particular, Wan et al. [12] analyzed the performance of a flamelet model with a premixed look-up table in the prediction of sodium emissions in coal combustion by comparing the results to DNS data. They pointed out that while the trends in conditional averages are captured, the concentrations of sodium oxides are under-predicted. It is not known whether tables based on non-premixed flamelets are able to circumvent this issue. In a wider view, there is no study on the validation of flamelet models for the prediction of K-species emissions in PBC.

Carrier-phase direct numerical simulation (CP-DNS) is a promising approach to determine the governing parameters of solid fuel combustion, examine associated sensitivities, and provide validation datasets for numerical modeling [13–15]. Wan et al. [16] conducted the 2D CP-DNS of pulverized corn straw for the investigation of K-species formation and their interaction with Cl- and S-species in an air atmosphere. They found that high strain rates help to enhance the transformation of KOH to K, $KHSO_4$ and K_2SO_4 while KCl is insensitive to the strain rate. While they used detailed K-Cl-S kinetics, the fuel composition was relatively simple without including heavy tars. Considering the complexity of biomass volatile content [17], a CP-DNS database with a more realistic fuel composition involving complex hydrocarbons as well as heavy tars seems necessary. Further, due to the mentioned distinct interaction of different K-species with the flow field, an extension of their work to a 3D setup to more accurately model the flow field strain/stretch processes is required.

The aim of this work is first, extending our fundamental knowledge on the physical aspects of alkali metal emissions in PBC. 3D CP-DNS of turbulent PBC in an oxy-fuel atmosphere with a detailed composition of biomass volatiles including heavy tars, obtained by the CRECK-S-B model [17], KOH, KCl, and SO_2 is carried out. Detailed homogeneous kinetics for both hydrocarbons and K-Cl-S containing species is considered, which to the best of the authors' knowledge, is done for the first time. Oxy-fuel atmosphere is considered since oxy-fuel combustion is deemed a promising technology for the energy transition and allows for the reduction of CO_2 emissions by means of carbon capture and storage. Pulverized walnut shells carried by a mixture of CO_2/O_2, are mixed with a surrounding hot environment in a temporally evolving jet setup and burn, which mimics the early stages of PBC. Combustion mode and chemical time scale analyses are performed to gain a better understanding of the complex chemistry involved. The second objective is a performance test and *a-priori* analysis of the flamelet model, which is extended to predict alkali metal formation in PBC.

Table 1
Ultimate analysis (UA), proximate analysis (PA), and lower heating value (LHV) of the walnut shells [22,23].

UA (wt%daf)				PA (wt%dry)	
C	55.04	N	1.54	Fixed carbon	37.9
H	6.79	S	0.1	volatiles	59.3
O	36.52			Ash	2.8
LHV [MJ/kg]			20.16		

2. Modeling

2.1. Carrier-phase DNS of PBC

The carrier gas phase is described in an Eulerian framework, while the biomass particles are treated in a Lagrangian framework with a point-particle approach. Mass, momentum, and energy transport equations are solved in a low-Mach number formulation for the gas phase. Since finite-rate chemistry is employed, individual species transport equations are solved, and the unity Lewis number assumption with a Prandtl number of 0.7 is invoked. Radiation is considered by the discrete ordinate method (DOM) using 16 directions. Absorption/emission coefficients are treated in a way similar to [18]. For the solid phase the mass, momentum and energy balance is considered as described below. The mass loss of particle reads $\mathrm{d}m_p = -(\dot{m}_{p,vol} + \dot{m}_{p,cog})\mathrm{d}t$, where the devolatilization mass loss is $\dot{m}_{p,v} = (m_{p,VM,0} - m_{p,VM})A\mathrm{e}^{-E/R_u T_p}$, with T_p, $m_{p,VM,0}$, and $m_{p,VM}$ the particle temperature, the initial and instantaneous mass of volatile matter, respectively, and the rate coefficients ($A = 7 \cdot 10^5$ [1/s], $E = 5 \cdot 10^7$ [J/Kmol]) are calculated by fitting to detailed kinetics as described in the next section. The overall char conversion rate ($\dot{m}_{p,cog}$) is calculated with Smith's intrinsic model [19] with an enhancement factor to account for the higher char reactivity of biomass [1]. With the assumption that the drag force is the dominant force on the particle, a non-spherical drag model with a shape factor of 0.75 is applied [20]. The particle temperature is governed by [10]

$$\frac{\mathrm{d}T_p}{\mathrm{d}t} = \frac{1}{\tau_{con}}(T - T_p) + \frac{\varepsilon_p A_p \sigma}{m_p c_{p,p}}(\Theta_r^4 - T_p^4) + \frac{\dot{Q}_{char}}{m_p c_{p,p}} + \frac{\dot{Q}_{devol}}{m_p c_{p,p}}, \tag{1}$$

where $\tau_{con} = \left(\mathrm{Pr}\rho_p d_p^2 c_{p,p}\right) / \left(6\mathrm{Nu}c_p\mu\right)$ is the convective heat transfer time scale [21], Nu the Nusselt number, and Pr the Prandtl number (= 0.7). μ and c_p are the gas viscosity and heat capacity at the particle position, respectively. d_p, ε_p and A_p are the particle diameter, emissivity and surface area, respectively. σ is the Stefan–Boltzmann constant, $c_{p,p}$ the heat capacity of the particle, expressed according to [18]. Θ is the Eulerian phase radiation temperature that is calculated with the DOM, and $\dot{Q}_{char}$ and $\dot{Q}_{devol}$ are the heat of char conversion and devolatilization, respectively [18]. The particle emissivity is initially $\varepsilon_p = 0.9$ and decreases linearly with char burnout to the ash emissivity (= 0.5) during char conversion. Char conversion is activated when $m_{p,VM}/m_{p,VM,0} = 0.9$ [18]. The two-way coupling between the two phases is governed by the exchange of mass from devolatilization and char processes, momentum from drag force, and enthalpy from radiation and convection, as well as the heat of devolatilization and char conversion, which have been described in detail elsewhere [10,18].

2.2. Fuel composition and gas-phase kinetics

The properties of the employed biomass are reported in Table 1. The ash analysis shows (by wt%) 2.20% SO_3, 6.20% P_2O_5, 9.90% SiO_2, 1.50% Fe_2O_3, 2.40% Al_2O_3, 16.60% CaO, 13.40% MgO, 1.00% Na_2O, 32.90% K_2O and 0.10% TiO_2 [23]. This corresponds to 0.7644 and 0.12936 wt% of K and Si by mass, respectively, in biomass which places walnut shells in a relatively low Si/K category [2]. The chlorine content

Table 2
Composition of walnut shell volatiles (wt%).

CO	13.4	CO_2	16.5
H_2O	8.4	H_2	0.34
CH_4	2.7	CH_2OHCHO	4.7
$C_6H_5OCH_3$	1.4	$C_6H_5OCH_3$	1.4
$C_6H_6O_3$	5.8	C_2H_5CHO	4.1
CH_3OH	4.1	CH_2O	1.8
$C_6H_{10}O_5$	5.8	C_2H_4	4.3
CH_3CO_2H	1.2	$C_5H_8O_4$	3.5
$C_{24}H_{28}O_4$	0.62	$C_5H_4O_2$	4.4
C_2H_5OH	0.45	CHOCHO	0.84
CH_3CHO	0.97	C_7H_8O	0.49
HOCHO	0.43	$C_8H_8O_3$	7.1
C_2H_3CHO	0.36	CH_2OHCH_2CHO	0.95
KOH	1.3	KCl	0.13
SO_2	0.26		

of 0.049 wt%(dry) places walnut shells in a low Cl/K category. Thus, it is assumed that at combustion relevant temperatures, K, Cl, and S content of the biomass is fully released [2]. The experiments in [2] show that a biomass with low Cl/K and Si/K releases a high portion of its K-Cl-S content at elevated temperatures. We refer to Si lean group (SL fuels in [2]), specifically oat (SL1) in Tab. 1 of [2] which has a similar ratio of Cl/K and Si/K as walnut shell. In Fig. 2b of [2] it is seen that at 1473 K 80% of K in oat is released. Similarly, Figs. 3b and 4b of [2] show 100% and 70% release of Cl and S, respectively. The release ratio increases with temperature as shown in these analyses. Thus, it is realistic to assume that K-Cl-S are fully released at flame temperatures that particles experience in the DNS.

The hydrocarbon (HC) species in the volatile matter and volatile yield are obtained by performing 0D simulations using a detailed multi-step devolatilization model, i.e., the CRECK-S-B model [17]. Specifically, the CRECK-S-B model is used in an *a-priori* manner considering different heating rates relevant for the current DNS setup. The resulting HC species are averaged to obtain the HC volatile species masses.

The K-Cl-S species are determined in another way on the basis of the elemental composition of biomass and its ash. Considering that the simulation is performed in high temperature combustion conditions, we have assumed that the released forms of K-Cl-S are KOH, KCl, and SO_2, which is a common assumption in such conditions and for this category of biomass [2,3,5,9]. By considering the molecular weight ratios, the K, Cl, and S content of biomass are converted to KOH, KCl, and SO_2 masses, respectively. When combined with HC species and normalized to one, we can obtain the full composition of volatile matter including K-Cl-S species that is reported in Table 2. This composition is held fixed and the fuel is released by a first order kinetic model with the rates obtained by fitting to the CRECK-S-B results. This means that following [8,12], the release rate of K-Cl-S species is considered the same as the one of the other volatile species. As mentioned in [12,16], the K-Cl-S vapor generated in the pores of particles is transported by the released volatile gases during the pyrolysis and so it is relevant to assume that their release rates are similar [12,16,24].

An automatic reduction code based on flux and sensitivity analyses [25] is used to reduce the detailed CRECK-G-2003 [26] hydrocarbon kinetics to a mechanism with 106 species and 2297 elementary reactions. To this end, atmospheric pressure, combustion-relevant temperatures and lean-to-rich equivalence ratios are selected as the operating range to sample reaction states. The reduction is targeted at retaining the accuracy of the gas-phase model in ignition delay times, flame temperature and flame speed considering the fuel mixture reported in Table 2. Next, the potassium, chlorine, and sulfur sub-mechanism [6] is combined with the reduced hydrocarbon mechanism. The resulting homogeneous kinetics involves 141 species and 2559 elementary reactions which is provided in the Supplementary Material. OpenSMOKE++ ODE solver [27] combined with a chemistry load balancing technique for large scale parallel computations is employed to efficiently integrate the resulting stiff ODE system.

2.3. Flamelet tabulation method

For a flamelet model to describe the emissions of K-Cl-S compounds from biomass flames, the mixture fractions for volatile matter Z_{vol} and char off-gases Z_{pro} [28] are considered to characterize the mixing between the fuel species and the oxidizer. To avoid numerical issues for the extraction from the flamelet look-up table (FLT), the flamelet solutions are mapped to a unit square space, i.e., $X = Z_{pro}/\left(Z_{vol} + Z_{pro}\right)$ and $Z = Z_{vol} + Z_{pro}$. To consider the gas species released by interphase mass transfer in the flamelet table, the 1D non-premixed flamelet equations are solved for different values of X. To consider the interphase heat transfer, the temperature boundaries of the flamelet equations are also varied, with the fuel temperature being set equal to the oxidizer temperature ($T_f = T_{ox}$) based on the findings of the detailed analysis of the pulverized coal combustion characteristics [29]. For ease of extraction from the flamelet table, the flamelet boundaries are mapped to the normalized total enthalpy space, which is defined as $H_{e,norm} = \left(H_e - H_{e,min}\right)/\left(H_{e,max} - H_{e,min}\right)$. Here, $H_{e,max}$ and $H_{e,min}$ are the maximum and minimum total enthalpies for specific values of X and Z. To consider the strain rate effects in the flamelet table, the scalar dissipation rate χ_{st} is varied from the equilibrium state to the extinction limit. Then, the parameter χ_{st} is transformed to reaction progress variable Y_{PV} space following the flamelet/progress variable (FPV) approach [30]. The progress variable is defined as $Y_{PV} = Y_{CO_2} + Y_{H_2O} + Y_{CO} + Y_{H_2}$ [31]. Finally, the thermo-chemical quantities, grouped as Ψ, in the flamelet table are parameterized as $\Psi = \mathcal{F}\left(X, Z, Y_{PV}, H_{e,norm}\right)$. In this work, the performance of the flamelet model in predicting the alkali species in a biomass flame is evaluated through an *a priori* analysis. In the *a priori* analysis, the trajectory variables X, Z, Y_{PV} and $H_{e,norm}$ are obtained from the DNS, and the tabulated values are compared to the reference DNS results. While Y_{PV} and $H_{e,norm}$ can be obtained directly from the species mass fractions and total enthalpy in the DNS, additional governing equations are solved for the mixture fractions of volatile matter Z_{vol} and char off-gases Z_{pro} in the DNS to facilitate flamelet tabulation. The reader is referred to [28] for the formulation of the governing equations.

3. Computational setup

Following our previous work [15], the computational domain is a 3D box with $L_x = 36\,\text{mm}$, $L_y = 48\,\text{mm}$, and $L_z = 24\,\text{mm}$, where x, y, and z are the stream-wise, cross-stream, and span-wise directions, respectively. A central jet of dry pulverized biomass particles in an oxy-fuel atmosphere consisting of $73\%CO_2/27\%O_2$ by volume [11] with an initial width of $H = 3.0\,\text{mm}$, a temperature of $T = 680\,\text{K}$ and a velocity of $U_x = 15\,\text{m/s}$ is mixed with an opposed-direction stream of hot gases with $U_x = -15\,\text{m/s}$ at 1680 K which are the products of biomass volatile-air combustion at $Z_{vol} = 0.0744$. Isotropic and divergence-free perturbations with 5% turbulence intensity and a length scale of $H/6$ are superimposed on the mean velocity to speed up the transition to a fully turbulent stage. The transition occurs at around $t = 20\,t_j$ with the jet time defined by $t_j = \Delta U/H = 0.1\,\text{ms}$. $\Delta U = 30\,\text{m/s}$ is the initial velocity difference between the two streams. The particle diameter is initially set to $d_p = 25\,\mu\text{m}$ [16] and decreases during char conversion. Depending on the seizing process, such particle sizes in PBC are achievable (5–46 μm) [32]. The particle size in the DNS considers the limitations of the point-particle assumption regarding the d_p/Δ_x ratio, the required mesh resolution to resolve the turbulence (Δ_x/η), and the flame structure [16]. The number density of the injected particles is $1.0 \cdot 10^{11}$ particles/m^3, typical for a pulverized solid fuel combustor. Initially, the particles with a density of $650\,\text{kg/m}^3$ [5] have the same velocity and temperature as the local carrier gas. The grid resolution is $100\,\mu\text{m}$ which results in 41,472,000 uniform-size computational cells. The mesh is fine enough to place at least 10 grid points across the flame front based on the OH profile, as well as to resolve all scales of turbulence. A low-Mach finite-volume reactive multiphase solver

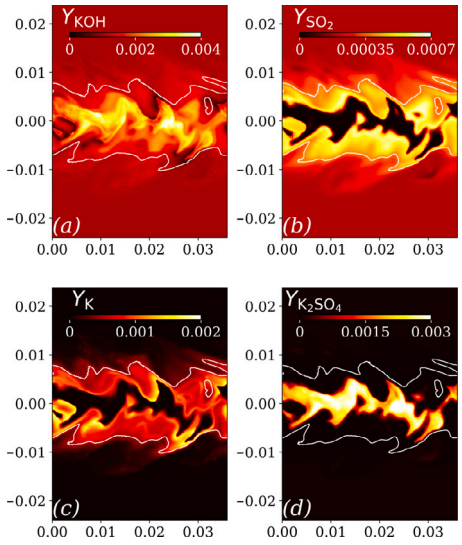

Fig. 1. Snapshots of **(a)** KOH, **(b)** SO_2, **(c)** K, and **(d)** K_2SO_4 mass fractions in the central x-z plane of the DNS domain at 3 ms ($30\,t_j$). Particles are removed for better illustrations. The white lines correspond to $Z_{vol,st}$ iso-lines.

similar to our previous works [15,33] is used. The simulation is carried out with a fixed computational time step of $5 \cdot 10^{-7}$ s until $t = 4$ ms corresponding to $40\,t_j$. We note that the time scale of the full PBC process including full char conversion is a few orders of magnitude larger than the $t = 4$ ms considered in the DNS. However, the current work focuses on early-stage events in PBC when release and combustion of volatiles from biomass is dominant. The maximum residence time in the DNS ($40\,t_j = 4$ ms) was set in such a way as to mimic the residence time of particles in the near quarl region of a swirl burner [11]. In Fig. 5e of [11] it is seen that volatiles are mostly released within and in the vicinity of the quarl zone up to about 80 mm below the quarl. With the gas velocity difference of 15 m/s near the injection zone [11], the estimated residence time is ≈5 ms which agrees with the DNS setup. The computational cost for $40\,t_j$ simulation of PBC in the current setup is approximately 2.35 M CPUh (72 h on 32,767 AMD-7742 cores) on the *Hawk* HPC at HLRS Stuttgart.

4. Results and discussion

4.1. Characterization of alkali metal formation

In Fig. 1a-d, snapshots of selected K-species and SO_2 are depicted at 3 ms ($30\,t_j$). This is the time when sufficient fuel has been released from the biomass particles and mixed with the surrounding oxidizer, such that a stoichiometric mixture fraction surface has established itself in the mixing layer, which is shown by the white iso-lines. In Fig. 1a and d, it can be seen that KOH and K_2SO_4 peak in the rich region inside the upper and lower flames, which are roughly aligned white iso-lines of $Z_{vol,st}$. Volatile-rich regions are common in pulverized coal/biomass burners. These mostly exist close to the burner in the quarl zone, where particles are rapidly heated by the recirculated volatile gases and combustion products [11]. Fig. 1b shows that SO_2 has its minimum amount in the region where K_2SO_4 peaks. It can also be observed that SO_2 and K have relatively high values in the volumes surrounding the region with high K_2SO_4.

We further analyze these behaviors by investigating K_2SO_4 profiles in Z space in Fig. 2, where instantaneous $Y_{K_2SO_4}$ versus mixture fraction is depicted. The points are colored by the reaction rate of K_2SO_4. As can be seen, at this stage of combustion, K_2SO_4 mainly forms in the rich mixture and is consumed toward the stoichiometry, where it reaches its minimum. The conditional average of the molar reaction rate of

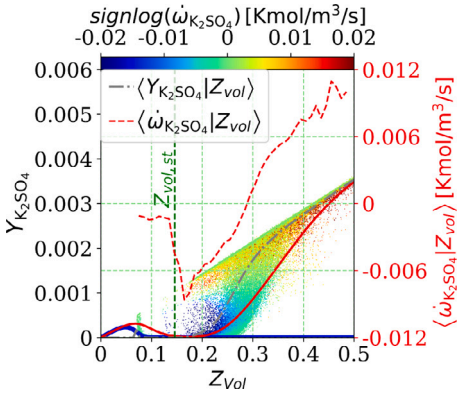

Fig. 2. Scatter plot of $Y_{K_2SO_4}$ vs. mixture fraction at 3 ms colored by reaction rate of K_2SO_4. Note that $signlog(\dot{\omega}_{K_2SO_4}) = sign(\dot{\omega}_{K_2SO_4}) \log_{10}(1 + |\dot{\omega}_{K_2SO_4}|)$ with $sign(.)$ the sign function, is used to distinguish the sign change of $\dot{\omega}_{K_2SO_4}$. Positive and negative values highlight K_2SO_4 formation and destruction regions, respectively. The red and gray dashed lines show conditional averages. The blue and red lines correspond to characteristic flamelets at minimum and maximum χ_{st}, respectively.

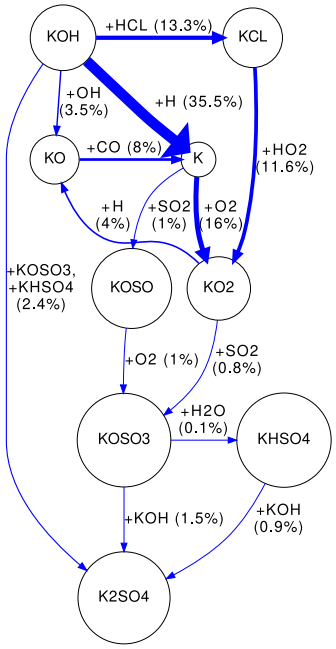

Fig. 3. Reaction path analysis conditioned on DNS cells where $\dot{\omega}_{K_2SO_4} > 0$ using the flux of element K. Percentages beside the arrows show the flux magnitude normalized by the sum of volume-averaged fluxes of K in the figure (= 0.254 Kmol/m³/s). Thickness of arrows is weighted by the corresponding normalized flux magnitudes.

K_2SO_4 viz. $\langle \dot{\omega}_{K_2SO_4}|Z_{vol}\rangle$ is shown as a red dashed line and provides an overall behavior of K_2SO_4 reaction rate. It shows that on average, the sign change of $\dot{\omega}_{K_2SO_4}$ i.e. formation to destruction of K_2SO_4 occurs in rich zones with $Z \approx 2Z_{vol,st}$. Characteristic flamelets show that at lower strain rates K_2SO_4 peaks at lean conditions (blue line), whereas at high strain rates, which are prevalent in the DNS, K_2SO_4 exists in a slightly higher amount on the lean side, is near-zero at stoichiometry, and progressively increases to its largest values on the rich side.

Alkali metal emissions are not available from experiments of turbulent PBC. Here, the qualitative agreement of DNS and characteristic flamelets at two distinctive scalar dissipation rates in Fig. 2 assure the reliability of the DNS. This is because single flamelets are mainly governed by the underlying kinetics which has been validated using experimental observations of K-Cl-S species interactions in pyrolysis and post flame conditions [4,7].

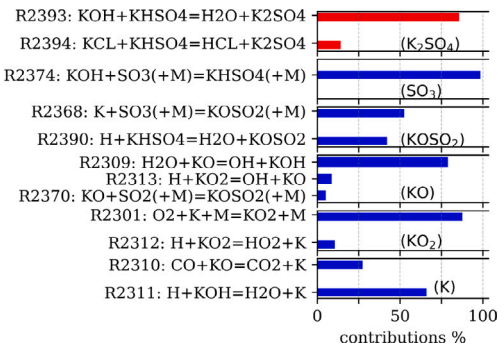

Fig. 4. Rate of production analysis conditioned on DNS cells where $\dot{\omega}_{K_2SO_4}$ is negative. Contributions are normalized by the sum of each species reaction rate. Red and blue colors show reactions contributing to more than 5% of the production and destruction of the relevant species, respectively.

In Fig. 3, we evaluate the formation pathway of K_2SO_4 by the conditional path-flux analysis, i.e., calculating the space-averaged flux of element K in regions of the DNS domain where $\dot{\omega}_{K_2SO_4} > 0$. The procedure for the evaluation of space-averaged production (destruction) pathways was described in [33] and is provided in the Supplementary Material as well. It can be seen that KOH is decomposed and produces K and KO through R2311: KOH+H→ H_2O+K, and R2309: KOH+OH→ H_2O + KO, respectively. The reaction numbers refer to the kinetics in the Supplementary Material. KO is converted to K by reaction with CO released by particles (R2310: KO + CO → CO_2 + K). K is converted to KO_2 by reaction with the available oxygen through the third-body reaction R2301: $K + O_2(+M) \rightarrow KO_2(+M)$. KCl, which is also present in the volatile matter, contributes to KO_2 production similarly to K (see the flux weights beside the arrows from K to KO_2 and from KCl to KO_2). Further, KO_2 contributes to K_2SO_4 formation through the production of $KOSO_3$ by reaction with the other volatile species, i.e., SO_2. SO_2 contribution to K_2SO_4 production involves another path, which is through the direct reaction with K and the production of KOSO. KOSO will then be converted to $KOSO_3$. Finally, $KOSO_3$ produces K_2SO_4 either directly, or indirectly through $KHSO_4$. We note that the contribution of SO_2 is different from what is normally considered. It is believed that in a cooling environment, SO_2 produces SO_3 by direct oxidation and that SO_3 further reacts with KOH and KCl to produce the precursors of K_2SO_4. The different active paths in the current simulation can be due to the abundance of K and KO_2 radicals with which SO_2 favors to react.

In Fig. 4, we analyze the fate of K_2SO_4 and the formation of other relevant species closer to the stoichiometric surface by the rate of production analysis, conditioned on regions with $\dot{\omega}_{K_2SO_4} < 0$. Note that the panel for K_2SO_4 in Fig. 4 shows the contributing reactions for the destruction of K_2SO_4 while for the other species, the contributing reactions for their production is shown. It can be seen that K_2SO_4 mainly converts to KOH, KCl, and $KHSO_4$ through backward reactions R2393 and R2394. Almost all SO_3 production can be associated with $KHSO_4$ through backward reaction R2374 (SO_3 panel). SO_3 and $KHSO_4$ are main contributors of $KOSO_2$ ($KOSO_2$ panel) which then partly produces KO through backward reaction R2370 (KO panel). Other KO contributors are KOH (R2309 backward) and KO_2 (R2313 forward). Note that KOH is a volatile species and was also produced by the destruction of K_2SO_4 as mentioned above. KO_2 has been mainly produced by K (KO_2 panel), and finally K has been mainly produced by KOH (K panel). It can be concluded that in regions away from the jet center toward the stoichiometry, the destruction of K_2SO_4 promotes alkali species formation. KCl, and KOH further produce K and KO_2.

The analysis in this section showed the formation of K_2SO_4 in highly strained, rich zones of the jet at relatively low temperatures. In [16], a similar behavior was predicted from 1D flamelets but not observed in the DNS. This is mainly due to the lean condition, as a result of the low particle number density that was considered in [16]. In fact, high concentrations of K_2SO_4 can be also achieved in 0D simulations (not shown for the sake of brevity) when rich mixtures ($Z > 0.3$ corresponding to $\phi > 2.5$) of the fuel and oxidizer at low temperatures ($T < 1300$ K) react within residence times of the order of a few milliseconds. This highlights the low-temperature chemistry effect in such conditions.

4.2. Evaluation of the flamelet approach

In Fig. 5, the comparison of the FPV results (markers) to the DNS data (lines) along a line across the flame at the middle x-z plane is shown. As shown in Fig. 5, temperature and light hydrocarbon species (Figs. 5a–b) and the main hydrocarbon volatile species, ethane (Fig. 5c) are predicted well across the jet. Fig. 5c shows that $C_8H_8O_3$, a representative tar species, is over-predicted in the center of the jet. In Figs. 5d–f, chlorine- and potassium-containing species are depicted. As illustrated in Fig. 5d, the Cl-containing species, HCl and KCl, are well predicted across the flame. Further, as shown in Figs. 5e–f, K-species mass fractions are reasonably predicted across y, although discrepancies can be observed in the central region where K, KOH, and $KHSO_4$ are over-predicted, while K_2SO_4 is notably under-predicted.

We further analyze the DNS data at 3 ms to investigate the reasons for the observed discrepancies. In Fig. 6 (top), averages of the chemical time scale ($\overline{\tau}_c$) of important species are depicted. The chemical time scale of the species is defined as the ratio of its concentration to its molar reaction rate and is calculated by the DNS data. Here, spatial averaging of a quantity q viz. $\overline{q}(y,t)$ is performed over homogeneous directions x and z. A Favre-averaged quantity is defined as $\tilde{q} = \overline{\rho q}/\overline{\rho}$ with ρ the density of the mixture. A large difference between the chemical time scales of $C_8H_8O_3$, KOH, and K_2SO_4 (in the order of milliseconds) and other species, i.e., CO, C_2H_6, and KCl, is observed in the central region. This is a rich zone (see the red dashed line), where temperature is lower than the temperature at stoichiometry (see the background color). Toward the stoichiometry, most of the processes become faster. Slow processes of oxidation of KOH, formation of K_2SO_4, and decomposition of heavy tars in this zone and notably faster combustion processes in the vicinity of the stoichiometry happen simultaneously, which affect the predictions via steady-state flamelets.

In Fig. 6 (bottom), we further investigate the combustion mode using the scatter data of the heat release rate colored by the flame index (FI) from the DNS. FI is defined as $FI = (\nabla F \cdot \nabla \mathrm{Ox})$ taking into account major hydrocarbon and alkali species as fuel (F) and O_2 as oxidizer (Ox). As can be seen, in the vicinity of the stoichiometry, non-premixed combustion mode is prevalent as the FI is negative. This explains the good performance of the flamelet model near the stoichiometric surface. However, in the richer regions a mixed combustion mode can be observed, which is identified by the scatter points having considerable heat release with negative and positive FI. This is due to the reaction of K-Cl-S species and heavy hydrocarbons mixed with O_2 in the center of the jet. The presence of such a mixed combustion mode may adversely affect the predictions of the non-premixed flamelet model.

To summarize this section, lighter hydrocarbons, including CO, C_2H_6, as well as KCl, show fast chemistry across the jet, while the major tar species ($C_8H_8O_3$) and K-species including, KOH, and K_2SO_4, show notably higher chemical time scales in the low-temperature rich zone. Furthermore, multiple combustion modes coexist. While the steady non-premixed flamelet model is able to accurately predict the composition space variables including K-species in regions with fast chemistry, to consider the transient effects and the multiple combustion modes, an unsteady multi-regime flamelet model for pulverized solid fuel combustion should be developed, extending earlier work from [34].

The scope of the current work is to generate a high-fidelity database with detailed kinetics to assess the flamelet modeling approach and gain a better understanding on the physical aspects of alkali metal

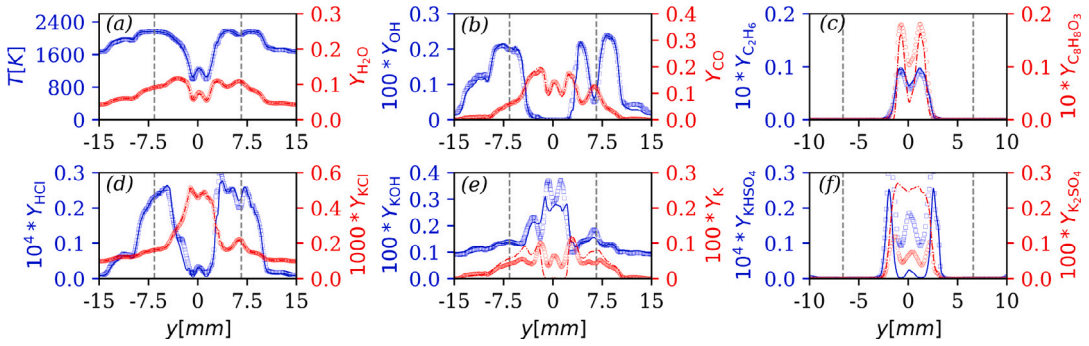

Fig. 5. Comparison of FPV predicted values (markers) and DNS (lines) at 3 ms along the y-direction at the center of the DNS domain. The vertical dashed line shows the location of Favre-averaged $Z_{vol,st}$.

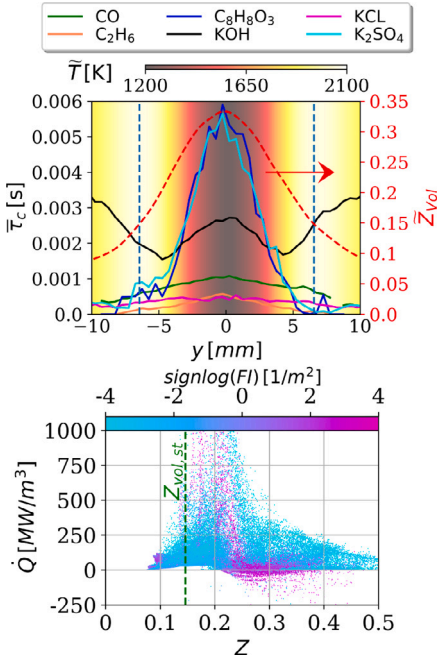

Fig. 6. (Top) Chemical time scale analysis at 3 ms. The vertical dashed lines show the location of $\widetilde{Z} = Z_{vol,st}$. The background color shows the Favre-averaged temperature. **(Bottom)** Scatter plot of heat release rate ($\dot{Q}$) in the Z space at 3 ms, colored by the flame index (FI). $signlog(FI)$ is used to highlight the sign change (see Fig. 2).

interactions in a turbulent flame and no parametric analysis has been performed. We believe that parameters such as particle number density, particle size, and turbulence do not influence the flamelet model's performance. However, they may affect the volatile flame formation and the alkali metals interactions. Given the high computational cost of the simulation, we leave the parametric studies for future work where we probably need to reduce the complexity of the kinetics to be able to do it with a reasonable computational cost.

5. Conclusions

3D CP-DNS of turbulent pulverized walnut shells combustion and the emissions of alkali metals in an oxy-fuel atmosphere with detailed kinetics is carried out. A detailed composition of biomass, including heavy tars, obtained by the CRECK-S-B model along with KOH, KCl, and SO_2, is considered as the fuel which is released by the particles during the turbulent mixing and particle heat up. The DNS results are analyzed and used in an *a-priori* assessment of the flamelet/progress variable (FPV) approach.

A predominantly non-premixed flame in the vicinity of the stoichiometric surface forms, while in the rich region in the center of the turbulent jet, premixed and non-premixed combustion modes co-exist. The released K-radicals from KOH and KCl react directly with SO_2 in the highly strained and rich regions, which yields large amounts of K_2SO_4. Closer to the flame surface, K_2SO_4, KCl, and KOH are consumed which lead to the production of K and KO_2.

Overall, the predictions of the flamelet model based on steady non-premixed flamelets show a good agreement with the DNS data. Specifically, temperature, light hydrocarbon species, as well as C_2H_6, and Cl-containing species (HCl and KCl) are well predicted across the jet, while $C_8H_8O_3$ is over-predicted in the center of the jet. K-species mass fractions are reasonably predicted across the flame except the center of the jet, where K, KOH, and $KHSO_4$ are over-predicted, while K_2SO_4 is under-predicted. This is partly due to the mixed combustion mode in this region, which affects the performance of the non-premixed flamelet table, and partly due to the slow kinetics for tar and K-species in this region. While CO, C_2H_6, and KCl show small time scales and their concentrations are close to the flamelet manifold, the chemical time scales of $C_8H_8O_3$, KOH, and K_2SO_4 are notably higher in the rich zone and such finite rate effects are difficult to capture with tabulated chemistry methods based on steady-state flamelets.

Novelty and Significance Statement

1. Pulverized biomass combustion (PBC), an appealing option for sustainable energy transition, is investigated. 2. This is the first 3D carrier-phase DNS of alkali metal emissions in turbulent PBC, with a detailed fuel composition for biomass volatiles and detailed kinetics with 141 species and 2559 reactions. 3. Oxy-fuel combustion, a promising technology to reduce CO2 emissions is considered. 4. The DNS data used for an a priori assessment of the predictions of a flamelet model in PBC.

CRediT authorship contribution statement

Ali Shamooni: Conceptualization, Methodology (CP-DNS), Software, Validation, Investigation, Formal analysis, Writing – original draft, Writing – review & editing. **Xu Wen:** Conceptualization, Methodology (flamelet model), Software, Validation, Formal analysis, Writing – review & editing. **Paulo Debiagi:** Methodology (solid-phase kinetics), Software, Validation, Writing – review & editing. **Alessandro Stagni:** Methodology (gas-phase kinetics), Software, Validation, Writing – review & editing. **Jan W. Gärtner:** Software (parallel simulation efficiency), Writing – review & editing. **Thorsten Zirwes:** Supervision, Writing – review & editing. **Oliver T. Stein:** Funding acquisition, Project administration, Supervision, Writing – review & editing. **Christan Hasse:** Funding acquisition, Project administration, Supervision, Writing – review & editing. **Andreas Kronenburg:** Funding acquisition, Project administration, Supervision, Writing – review & editing.

Declaration of competing interest

The authors declare that they have no known competing financial interests or personal relationships that could have appeared to influence the work reported in this paper.

Acknowledgments

The authors acknowledge the financial support by the German Research Foundation (DFG) project No. 513858356, and No. 215035359 (CRC/Transregio 129 Oxy-flame). O. T. Stein acknowledges the financial support by the Helmholtz Association of German Research Centers (HGF), Germany, within the research field Energy, program Materials and Technologies for the Energy Transition (MTET), topic Resource and Energy Efficiency. HPC resources are provided by HLRS Stuttgart. We thank Prof. Peter Glarborg for helpful discussions on the alkali kinetics.

Appendix A. Supplementary data

Supplementary data associated with this article are the homogeneous kinetics and the procedure to perform space-averaged reaction path flux analysis.

Supplementary material related to this article can be found online at https://doi.org/10.1016/j.proci.2024.105309.

References

[1] A. Williams, J. Jones, L. Ma, M. Pourkashanian, Pollutants from the combustion of solid biomass fuels, Prog. Energy Combust. Sci. 38 (2) (2012) 113–137.
[2] J.N. Knudsen, P.A. Jensen, K. Dam-Johansen, Transformation and release to the gas phase of Cl, K, and S during combustion of annual biomass, Energy Fuels 18 (5) (2004) 1385–1399.
[3] M.R. Mortensen, H. Hashemi, H. Wu, P. Glarborg, Modeling post-flame sulfation of KCl and KOH in bio-dust combustion with full and simplified mechanisms, Fuel 258 (2019) 116147.
[4] A. Chanpirak, M.K.K. Jensen, H. Wu, P. Glarborg, Sulfation of gaseous KCl by H_2SO_4, Energy Fuels 37 (3) (2023) 2319–2328.
[5] H. Fatehi, Z. Li, X. Bai, M. Aldén, Modeling of alkali metal release during biomass pyrolysis, Proc. Combust. Inst. 36 (2017) 2243–2251.
[6] W. Weng, S. Chen, H. Wu, P. Glarborg, Z. Li, Optical investigation of gas-phase KCl/KOH sulfation in post flame conditions, Fuel 224 (2018) 461–468.
[7] E. Thorin, K. Zhang, D. Valiev, F.M. Schmidt, Simultaneous detection of K, KOH, and KCl in flames and released from biomass using photofragmentation TDLAS, Opt. Express 29 (26) (2021) 42945.
[8] L. Ma, J. Jones, M. Pourkashanian, A. Williams, Modelling the combustion of pulverized biomass in an industrial combustion test furnace, Fuel 86 (12–13) (2007) 1959–1965.
[9] S.M. Mousavi, E. Thorin, F.M. Schmidt, A. Sepman, X.-S. Bai, H. Fatehi, Numerical study and experimental verification of biomass conversion and potassium release in a 140 kW entrained flow gasifier, Energy Fuels 37 (2) (2023) 1116–1130.
[10] T.D. Luu, A. Shamooni, O.T. Stein, A. Kronenburg, S. Popp, H. Nicolai, H. Schneider, X. Wen, C. Hasse, Flame characterisation of gas-assisted pulverised coal combustion using FPV-LES, Proc. Combust. Inst. 39 (3) (2023) 3249–3258.
[11] X. Wen, H. Nicolai, P. Debiagi, D. Zabrodiec, A. Maßmeyer, R. Kneer, C. Hasse, Flamelet LES of a 40 kWth pulverized torrefied biomass furnace in air and oxy-fuel atmospheres, Proc. Combust. Inst. 39 (4) (2023) 4563–4572.
[12] K. Wan, L. Vervisch, J. Xia, P. Domingo, Z. Wang, Y. Liu, K. Cen, Alkali metal emissions in an early-stage pulverized-coal flame: DNS analysis of reacting layers and chemistry tabulation, Proc. Combust. Inst. 37 (3) (2019) 2791–2799.
[13] K. Luo, H. Wang, J. Fan, F. Yi, Direct numerical simulation of pulverized coal combustion in a hot vitiated co-flow, Energy Fuels 26 (10) (2012) 6128–6136.
[14] T. Hara, M. Muto, T. Kitano, R. Kurose, S. Komori, Direct numerical simulation of a pulverized coal jet flame employing a global volatile matter reaction scheme based on detailed reaction mechanism, Combust. Flame 162 (12) (2015) 4391–4407.
[15] X. Wen, A. Shamooni, H. Nicolai, O.T. Stein, A. Kronenburg, A.M. Kempf, C. Hasse, Flame structure analysis and flamelet modeling of turbulent pulverized solid fuel combustion with flue gas recirculation, Proc. Combust. Inst. 39 (3) (2023) 3409–3418.
[16] K. Wan, Z. Wang, J. Xia, L. Vervisch, P. Domingo, Y. Lv, Y. Liu, Y. He, K. Cen, Numerical study of HCl and SO_2 impact on potassium emissions in pulverized-biomass combustion, Fuel Process. Technol. 193 (2019) 19–30.
[17] P. Debiagi, G. Gentile, A. Cuoci, A. Frassoldati, E. Ranzi, T. Faravelli, A predictive model of biochar formation and characterization, J. Anal. Appl. Pyrolysis 134 (2018) 326–335.
[18] M. Rieth, A.M. Kempf, A. Kronenburg, O.T. Stein, Carrier-phase DNS of pulverized coal particle ignition and volatile burning in a turbulent mixing layer, Fuel 212 (2018) 364–374.
[19] I.W. Smith, The combustion rates of coal chars: A review, Sympos. (Int.) Combust. 19 (1) (1982) 1045–1065.
[20] R. Backreedy, L. Fletcher, J. Jones, L. Ma, M. Pourkashanian, A. Williams, Co-firing pulverised coal and biomass: a modeling approach, Proc. Combust. Inst. 30 (2) (2005) 2955–2964.
[21] W.E. Ranz, J. Marshall, Evaporation from drops - Part 1, Chem. Eng. Prog. 48 (3) (1952) 141–146.
[22] A. Demirbaş, Fuel characteristics of olive husk and walnut, hazelnut, sunflower, and almond shells, Energy Sources 24 (3) (2002) 215–221.
[23] Phyllis2, database for (treated) biomass, algae, feedstocks for biogas production and biochar, TNO biobased and circular technologies, 2023, https://phyllis.nl/Biomass/View/2318. (Accessed September 2023).
[24] Y. Liu, Z. Wang, J. Xia, L. Vervisch, K. Wan, Y. He, R. Whiddon, H. Bahai, K. Cen, Measurement and kinetics of elemental and atomic potassium release from a burning biomass pellet, Proc. Combust. Inst. 37 (3) (2019) 2681–2688.
[25] A. Stagni, A. Frassoldati, A. Cuoci, T. Faravelli, E. Ranzi, Skeletal mechanism reduction through species-targeted sensitivity analysis, Combust. Flame 163 (2016) 382–393.
[26] G. Bagheri, E. Ranzi, M. Pelucchi, A. Parente, A. Frassoldati, T. Faravelli, Comprehensive kinetic study of combustion technologies for low environmental impact: MILD and OXY-fuel combustion of methane, Combust. Flame 212 (2020) 142–155.
[27] A. Cuoci, A. Frassoldati, T. Faravelli, E. Ranzi, OpenSMOKE++: An object-oriented framework for the numerical modeling of reactive systems with detailed kinetic mechanisms, Comput. Phys. Comm. 192 (2015) 237–264.
[28] X. Wen, H. Wang, Y. Luo, K. Luo, J. Fan, Evaluation of flamelet/progress variable model for laminar pulverized coal combustion, Phys. Fluids 29 (8) (2017).
[29] X. Wen, K. Luo, H. Wang, Y. Luo, J. Fan, Analysis of pulverized coal flame stabilized in a 3D laminar counterflow, Combust. Flame 189 (2018) 106–125.
[30] C.D. Pierce, P. Moin, Progress-variable approach for large-eddy simulation of non-premixed turbulent combustion, J. Fluid Mech. 504 (2004) 73–97.
[31] M. Ihme, L. Shunn, J. Zhang, Regularization of reaction progress variable for application to flamelet-based combustion models, J. Comput. Phys. 231 (23) (2012) 7715–7721.
[32] D. Zabrodiec, A. Massmeyer, J. Hees, O. Hatzfeld, R. Kneer, Flow pattern and behavior of 40 kWth pulverized torrefied biomass flames under atmospheric and oxy-fuel conditions, Renew. Sustain. Energy Rev. 138 (2021) 110493.
[33] A. Shamooni, P. Debiagi, B. Wang, T.D. Luu, O.T. Stein, A. Kronenburg, G. Bagheri, A. Stagni, A. Frassoldati, T. Faravelli, A.M. Kempf, X. Wen, C. Hasse, Carrier-phase DNS of detailed NO_x formation in early-stage pulverized coal combustion with fuel-bound nitrogen, Fuel 291 (2021) 119998.
[34] X. Wen, M. Rieth, W. Han, J.H. Chen, C. Hasse, Investigation of the ignition processes of a multi-injection flame in a Diesel engine environment using the flamelet model, Proc. Combust. Inst. 38 (4) (2021) 5605–5613.